

Synthetic magnetism enhanced mechanical squeezing in Brillouin optomechanical system

D. R. Kenigoule Massemblele,¹ P. Djourwé,^{1,2,*} Souvik Agasti,^{3,4} K.S. Nisar,⁵ A.K. Sarma,^{6,†} and A.H. Abdel-Aty⁷

¹*Department of Physics, Faculty of Science, University of Ngaoundere, P.O. Box 454, Ngaoundere, Cameroon*

²*Stellenbosch Institute for Advanced Study (STIAS), Wallenberg Research Centre at Stellenbosch University, Stellenbosch 7600, South Africa*

³*IMOMECE division, IMEC, Wetenschapspark 1, B-3590 Diepenbeek, Belgium*

⁴*Institute for Materials Research (IMO), Hasselt University, Wetenschapspark 1, B-3590 Diepenbeek, Belgium*

⁵*Department of Mathematics, College of Science and Humanities in Alkharj,*

Prince Sattam Bin Abdulaziz University, Alkharj 11942, Saudi Arabia

⁶*Department of Physics, Indian Institute of Technology Guwahati, Guwahati 781039, India*

⁷*Department of Physics, College of Sciences, University of Bisha, Bisha 61922, Saudi Arabia*

We propose a scheme to generate large amount of mechanical squeezing, far beyond the 3dB limit, which is based on synthetic magnetism in optomechanical system that hosts a Backward Stimulated Brillouin Scattering (BSBS) process. Our benchmark system consists of an acoustic mode coupled to two optical modes through the BSBS process, and a Duffing mechanical oscillator that couples to the same optical modes through the standard optomechanical radiation pressure. The synthetic magnetism comes from the modulation of the mechanical coupling between the acoustic and the mechanical mode. When there is no synthetic magnetism, a given amount of mechanical squeezing is generated in the system. This squeezing is mainly dependent on the BSBS process, and it is fragile against thermal noise. By switching on the synthetic magnetism, the degree of the generated squeezing is greatly enhanced and goes far beyond the limit of the 3dB. This large magnetism induced squeezing persists even when there is no BSBS process in the system. Moreover, this generated squeezing is robust enough against thermal noise in comparison to the one induced when the synthetic magnetism is off. Furthermore, both the mechanical variance squeezing and effective phonon number exhibit series of peaks and dips depending on the phase modulation of the mechanical coupling. This oscillatory feature is reminiscent of a sudden death and revival of squeezing phenomenon, which can be used to maintain a desired magnitude of squeezing by tuning this phase. Our proposal provides a path toward a flexible scheme that generates large amount of squeezing, far beyond the 3dB limit. Such a generated squeezed states can be used for quantum applications including quantum information processing, quantum sensing and metrology, and quantum computing.

Keywords: Optomechanics, synthetic magnetism, squeezing, Brillouin Scattering

I. INTRODUCTION

Nonclassical states such as squeezed and entangled states are crucial ingredients required to improve a range of quantum applications including quantum information processing [1–3], quantum sensing and metrology [4–7], quantum computing [8], and quantum supremacy [9–11]. For instance, entangled states have been widely generated in optomechanical systems [12, 13] by exploring diverse techniques [14–18], and they were recently proposed as resources to enhance sensing [19, 20]. Beside that, large intracavity squeezed field have been generated [21, 22], which can be used for mechanical cooling [23, 24], gravitational wave detection [25, 26], and to further generate nonclassical states [27]. Similarly, strong mechanical squeezed states [28] were equally generated, which can be useful to enhance mass-sensing [29–31], information processing [32, 33], and state transfer [34] involving phonons. Despite these interesting applications related to squeezed states, their generation is often limited by quantum noise that resists any measurement below the Zero Point Fluctuation (ZPF), i.e., beyond the 3dB limit. The existing systems in which mechanical squeezing beyond 3dB have been achieved have explored reservoir engineering technique

or two-tone driving [35–37].

Recently, technique based on synthetic magnetism (engineered via a modulation of the photon/phonon hopping rate) have been used in optomechanical structures for specific purposes. For instance, an artificial magnetic field for photons was engineered to achieve photon transport as reported in [38, 39]. Similarly, synthetic magnetic field for phonon/acoustic has been created [40–42] for phononic transport at the nanoscale. More recently, synthetic magnetism has been engineered in optomechanical systems to enhance entangled states generation [43]. Owing to these interesting physics fostered by synthetic magnetism in optomechanics, here we use it to enhance mechanical squeezing in optomechanical system involving Backward Stimulated Brillouin Scattering (BSBS) process which has been proposed in [44].

The underlying system, we are considering, consists of an acoustic (mechanical) mode coupled to two optical modes through the BSBS process (radiation pressure coupling). We propose a scheme to connect the acoustic and the mechanic modes through a mechanical coupling having a strength J_m that is modulated via a phase θ . Such a phase modulation of the coupling induces a synthetic magnetism in our model system [43, 45]. When the synthetic magnetism is switched off, a given amount of mechanical squeezing is generated in the system. This squeezing is mainly dependent on the BSBS process, and it is fragile against thermal noise [44]. By switching on the synthetic magnetism, we found that i) the degree of the generated squeezing is greatly enhanced and goes far

*Electronic address: djourwepp@gmail.com

†Electronic address: aksarma@iitg.ac.in

beyond the limit of the 3dB, ii) this squeezing persists even when there is no BSBS process in the system, and iii) this generated squeezing is robust enough against thermal noise in comparison to the case when the synthetic magnetism is off. Furthermore, both the mechanical squeezing and effective phonon number exhibit series of peaks and dips depending on the phase modulation of the mechanical coupling. This oscillatory feature induces a sudden death and revival of squeezing, which can be used to maintain a desired magnitude of squeezing by tuning the phase. Our proposal paves a way towards a flexible scheme that can be used to generate arbitrary amount of squeezing. Such a generated squeezed states can be used for quantum applications including quantum information processing, quantum sensing/metrology, and quantum computing.

The rest of our work is organized as follow. [section II](#) provides the dynamical equations and derives the analytical expressions involved in our investigation. The squeezing enhancement, together with the important results are presented throughout [section III](#). Our work is concluded in [section IV](#).

II. MODEL AND DYNAMICAL EQUATIONS

We consider a system consisting of an acoustic mode (b_a) that couples to two optical modes through the BSBS process, and a nonlinear mechanical oscillator (b_m) that couples also to the two optical modes. In order to enhance the squeezing of the mechanical oscillator, the acoustic and the mechanical modes are mechanically coupled, having coupling strength J_m . The coupling is modulated through a phase θ that induces a synthetic gauge into the dynamics. The Hamiltonian of such a system is given by ($\hbar = 1$):

$$H = H_0 + H_{\text{OM}} + H_{\text{BSBS}} + H_{\text{int}} + H_{\text{drive}}, \quad (1)$$

where

$$H_0 := \sum_{j=1,2} \omega_{c_j} a_j^\dagger a_j + \omega_a b_a^\dagger b_a + \omega_m b_m^\dagger b_m, \quad (2)$$

$$H_{\text{OM}} := \sum_{j=1,2} g_{a,m} a_j^\dagger a_j (b_m + b_m^\dagger) + \frac{\eta}{2} (b_m + b_m^\dagger)^4, \quad (3)$$

$$H_{\text{BSBS}} := -g_a (a_1^\dagger a_2 b_a + a_1 a_2^\dagger b_a^\dagger), \quad (4)$$

$$H_{\text{int}} := J_m (e^{i\theta} b_a^\dagger b_m + e^{-i\theta} b_a b_m^\dagger) \quad (5)$$

$$H_{\text{drive}} := \sum_{j=1,2} iE_j (a_j^\dagger e^{-i\omega_{p_j} t} - a_j e^{i\omega_{p_j} t}). \quad (6)$$

In the above Hamiltonian, the first term H_0 is the free Hamiltonian corresponding to the optical (a_j), the acoustic (b_a) and the mechanical (b_m) mode. The first term in H_{OM} captures the optomechanical interaction between the optical and the mechanical modes, while the second one accounts for nonlinear effect on the mechanical resonator through the Duffing coefficient η . The third term H_{BSBS} stands for the triply resonant phonon-photon interaction triggered via the BSBS process. H_{int} describes the mechanical coupling between the acoustic and the mechanical modes. The single-photon optomechanical (Brillouin) coupling, g_m (g_a), results from the radiation

pressure (electrostrictive) force. The last term, H_{drive} , denotes the drivings fields. Here E_j and ω_{p_j} are the amplitude and the frequency of the j^{th} field. In what follows, we will assume the same frequency field, $\omega_{p_{1,2}} \equiv \omega_p$. The optical cavity frequency are ω_{c_j} and the mechanical (acoustic) frequency is ω_m (ω_a). In the frame rotating at $H_r = \omega_{p_1} a_1^\dagger a_1 + \omega_{p_2} a_2^\dagger a_2 + (\omega_{p_1} - \omega_{p_2}) b_a^\dagger b_a$, the Hamiltonian in [Equation 1](#) becomes

$$H' = -\Delta_1 a_1^\dagger a_1 + \Delta_a b_a^\dagger b_a + \omega_m b_m^\dagger b_m - g_m a_1^\dagger a_1 (b_m + b_m^\dagger) + J_m (e^{i\theta} b_a^\dagger b_m + e^{-i\theta} b_a b_m^\dagger) + \frac{\eta}{2} (b_m + b_m^\dagger)^4 + iE_1 (a_1^\dagger - a_1) - G_a (a_1^\dagger b_a + a_1 b_a^\dagger), \quad (7)$$

where we have defined $\Delta_1 = \omega_{p_1} - \omega_{c_1}$, and $\Delta_a = \omega_a + \omega_{p_2} - \omega_{p_1}$. Here α_2 is the steady-state of the control optical mode a_2 , which has been treated classically as it is assumed to be strong compared to the weak strength of the Brillouin acoustic mode b_a (see details in [Appendix A](#)).

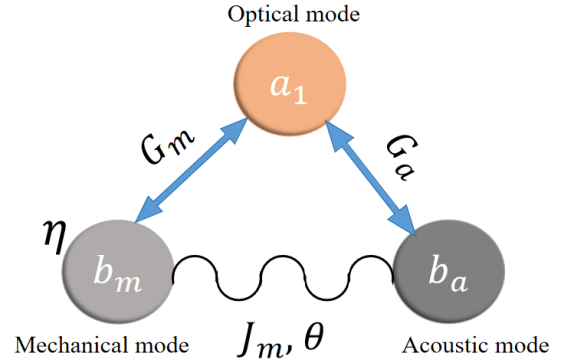


FIG. 1: Sketch of our linearized three mode optomechanical system. The mode a_1 is coupled to the acoustic (b_a) and the mechanical mode (b_m) with coupling strength G_a and G_m respectively. The mechanical oscillator has the Duffing coefficient η . The phonon-phonon hopping rate J_m is modulated by the phase θ .

By following the standard linearization procedure ([Appendix A](#)), the Hamiltonian in [Equation 7](#) can be linearized, and that reduces our scheme to a three-mode optomechanical system as depicted in [Figure 1](#). In order to investigate the squeezing of the mechanical resonator b_m , we introduce the following Bogoliubov transformation,

$$b_m = b_m^s \cosh(r) - b_m^{s\dagger} \sinh(r), \quad (8)$$

with the defined squeezing parameter $r = \frac{1}{4} \ln(1 + \frac{2\Lambda}{\omega_m})$ and the squeezed mechanical mode b_m^s . This transformation leads to the new linearized Hamiltonian,

$$H_{\text{lin}}^s = -\tilde{\Delta} \delta a_1^\dagger \delta a_1 + \Delta_a \delta b_a^\dagger \delta b_a + \omega'_m \delta b_m^{s\dagger} \delta b_m^s - (G'_m \delta a_1^\dagger + G'_m{}^* \delta a_1) (\delta b_m^{s\dagger} + \delta b_m^s) + J'_m (e^{i\theta} \delta b_a^\dagger \delta b_m^s + e^{-i\theta} \delta b_a \delta b_m^{s\dagger}) - G_a (\delta a_1^\dagger \delta b_a + \delta a_1 \delta b_a^\dagger), \quad (9)$$

with the effective parameters $\omega'_m = \sqrt{\omega_m(\omega_m + 2\Lambda)}$, $G'_m = G_m e^{-r}$ and $J'_m = J_m \cosh(r)$. The effective mechanical coupling is $G_m = g_m \alpha_1$, where $\Lambda = 24\eta \Re(\beta_m)^2$. β_m (α_1) is the steady-state of the mechanical (optical) mode.

By taking into account the dissipation associated with the optical (κ), the mechanical (γ_m) and the acoustic (γ_a) modes, one can obtain the following equations describing the dynamics of the fluctuations operators,

$$\begin{cases} \delta\dot{a}_1 = (i\tilde{\Delta} - \frac{\kappa}{2})\delta a_1 + iG'_m(\delta b_m^{s\dagger} + \delta b_m^s) + iG_a\delta b_a \\ \quad + \sqrt{\kappa}a_1^{in} \\ \delta\dot{b}_a = -(\frac{\gamma_a}{2} + i\Delta_a)\delta b_a - iJ'_m e^{i\theta}\delta b_m^s + iG_a\delta a_1 \\ \quad + \sqrt{\gamma_a}b_a^{in} \\ \delta\dot{b}_m^s = -(\frac{\gamma_m}{2} + i\omega'_m)\delta b_m^s - iJ'_m e^{-i\theta}\delta b_a + i(G'_m\delta a_1 \\ \quad + G'_m\delta a_1^\dagger) + \sqrt{\gamma_m}b_m^{sin}, \end{cases} \quad (10)$$

where $\tilde{\Delta} = \Delta - 2g_m \text{Re}(\beta_m)$ is the effective detuning. In the set of Equation 10, a_1^{in} , b_a^{in} and b_m^{sin} are zero-mean noise operators characterized by the following auto-correlation functions,

$$\begin{aligned} \langle a_1^{in}(t)a_1^{in\dagger}(t') \rangle &= \delta(t-t'), & \langle a_1^{in\dagger}(t)a_1^{in}(t') \rangle &= 0, \\ \langle b_a^{in}(t)b_a^{in\dagger}(t') \rangle &= \delta(t-t'), & \langle b_a^{in\dagger}(t)b_a^{in}(t') \rangle &= 0, \\ \langle b_m^{sin}(t)b_m^{sin\dagger}(t') \rangle &= (n_{th} \cosh(2r) + \sinh^2(r))\delta(t-t'), \\ \langle b_m^{in}(t)b_m^{in}(t') \rangle &= (n_{th} + \frac{1}{2})\sinh(2r)\delta(t-t'). \end{aligned} \quad (11)$$

Here, n_{th} represents the equilibrium phonon occupation number of the mechanical resonator, and is defined as, $n_{th} = [\exp(\frac{\hbar\omega_m}{k_b T}) - 1]^{-1}$, where k_b is the Boltzmann constant. Owing to the high-frequency acoustic mode b_a compared to the mechanical one ($\omega_m \ll \omega_a$) the thermal acoustic phonon occupation has been neglected. In order to investigate the effect of the mechanical coupling J_m and its phase modulation θ on squeezing of the targeted mechanical resonator, we first define the following amplitude (position) and phase (momentum) quadrature operators: $\delta X_\theta = \frac{\delta\mathcal{O}^\dagger + \delta\mathcal{O}}{\sqrt{2}}$, $\delta Y_\theta = i\frac{\delta\mathcal{O}^\dagger - \delta\mathcal{O}}{\sqrt{2}}$, with $\mathcal{O} \equiv a_1, b_a, b_m^s$. Similarly, the related noise quadratures read as: $\delta X_\theta^{in} = \frac{\delta\mathcal{O}^{in\dagger} + \delta\mathcal{O}^{in}}{\sqrt{2}}$, $\delta Y_\theta^{in} = i\frac{\delta\mathcal{O}^{in\dagger} - \delta\mathcal{O}^{in}}{\sqrt{2}}$. This enables us to derive the set of equations describing the quadrature dynamics of our system as,

$$\dot{u} = Mu + z^{in}. \quad (12)$$

Here $u = (\delta X_{a_1}, \delta Y_{a_1}, \delta X_{b_a}, \delta Y_{b_a}, \delta X_{b_m}, \delta Y_{b_m})^T$, $z^{in} = (\sqrt{\kappa}X_{a_1}^{in}, \sqrt{\kappa}Y_{a_1}^{in}, \sqrt{\gamma_a}X_{b_a}^{in}, \sqrt{\gamma_a}Y_{b_a}^{in}, \sqrt{\gamma_m}X_{b_m}^{in}, \sqrt{\gamma_m}Y_{b_m}^{in})^T$ and the matrix M is given by,

$$M = \begin{pmatrix} -\frac{\kappa_1}{2} & -\tilde{\Delta} & 0 & -G_a & 0 & 0 \\ \tilde{\Delta} & -\frac{\kappa_1}{2} & G_a & 0 & 2G'_m & 0 \\ 0 & -G_a & -\frac{\gamma_a}{2} & \Delta_a & J'_m \sin \theta & J'_m \cos \theta \\ G_a & 0 & -\Delta_a & -\frac{\gamma_a}{2} & -J'_m \cos \theta & J'_m \sin \theta \\ 0 & 0 & -J'_m \sin \theta & J'_m \cos \theta & -\frac{\gamma_m}{2} & \omega'_m \\ 2G'_m & 0 & -J'_m \cos \theta & -J'_m \sin \theta & -\omega'_m & -\frac{\gamma_m}{2} \end{pmatrix}, \quad (13)$$

Here the effective couplings G'_m and G_a have been assumed to be real for simplicity.

III. SYNTHETIC MAGNETISM ENHANCED MECHANICAL SQUEEZING

To illustrate the enhancement of the mechanical squeezing in our proposed scheme, we need to derive the position variance of the nonlinear mechanical resonator. For this purpose, we evaluate the covariance matrix, V_{ij} , where $V_{ij} = \frac{\langle u_i u_j + u_j u_i \rangle}{2}$. The covariance matrix satisfies the equation of motion,

$$\dot{V} = MV + VM^T + D, \quad (14)$$

with the diagonal diffusion matrix $D = \text{Diag}[\frac{\kappa}{2}, \frac{\kappa}{2}, \frac{\gamma_a}{2}, \frac{\gamma_a}{2}, \frac{\gamma_m}{2}e^{2r}(2n_{th} + 1), \frac{\gamma_m}{2}e^{-2r}(2n_{th} + 1)]$, and the matrix M must meet the Routh-Hurwitz stability criterion where all its eigenvalues should have negative real parts. The parameters are chosen in such a way that this stability criterion is met and they are experimentally feasible. As we aim to study the steady-state behavior of the mechanical squeezing, we use the long time limit of Equation 14 which is known as the Lyapunov equation,

$$MV + VM^T = -D. \quad (15)$$

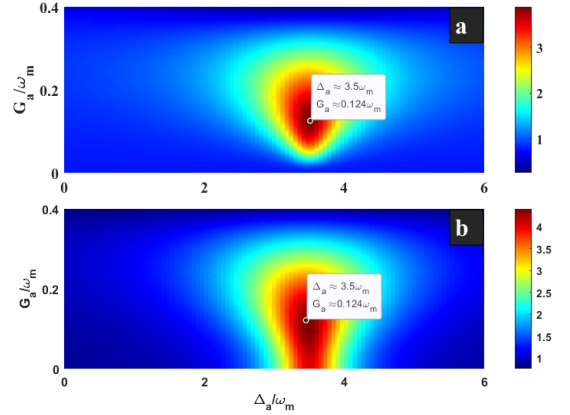


FIG. 2: Mechanical position variance from Equation 17 versus G_a and Δ_a . The mechanical coupling strength is $J_m = 0$ for (a) and $J_m = 0.1\omega_m$ for (b). The parameters used are $\omega_m/2\pi = 1\text{MHz}$, $g_m = 10^{-4}\omega_m$, $\kappa = 0.02\omega_m$, $\gamma_a = 0.4\omega_m$, $\gamma_m = 10^{-4}\omega_m$, $\eta = 10^{-4}\omega_m$, $n_{th} = 100$, $G_m = 0.15\omega_m$, $\tilde{\Delta} = -\omega'_m$, and $\theta = \pi/2$.

From the V_{ij} elements, we can obtain the position variance ($\langle \delta q_m^2 \rangle$) of the mechanical resonator as follows:

$$\langle \delta q_m^2 \rangle = V_{55} e^{-2r}, \quad (16)$$

which can be expressed in dB units as,

$$\langle \delta q_m^2 \rangle (dB) = -10 \log_{10} \frac{\langle \delta q_m^2 \rangle}{\langle \delta q_{ZPF}^2 \rangle}, \quad (17)$$

where $\langle \delta q_{ZPF}^2 \rangle = \frac{1}{2}$ is the zero-point fluctuations of the mechanical resonator. One can clearly see that the position

quadrature is getting squeezed. In order to effectively suppress the thermal effects at the the optimal acoustic resonance Δ_a^{opt} , as depicted in the terms, $G'_m(\delta a_1^\dagger \delta b_m^{\dagger s} + \delta a_1 \delta b_m^s)$, we work in the red-detuned regime ($\tilde{\Delta} = -\omega'_m$). The main parameters used for our numerical simulations are $\omega_m/2\pi = 1\text{MHz}$, $g_m = 10^{-4}\omega_m$, $\kappa = 0.02\omega_m$, $\gamma_a = 0.4\omega_m$, $\gamma_m = 10^{-4}\omega_m$, $\eta = 10^{-4}\omega_m$, $n_{th} = 100$, $G_m = 0.15\omega_m$, and $\tilde{\Delta} = -\omega'_m$. The other parameters such as J_m , θ , G_a and Δ_a are adjusted as latter on indicated on the related figures. Figure 2 exhibits the position variance as a function of the the acoustic effective coupling G_a and detuning Δ_a . It can be observed that the largest squeezing is generated at the acoustic resonance $\Delta_a^{\text{opt}} \approx 3.5\omega_m$ and $G_a = 0.124\omega_m$. For the rest of the work, we take $\Delta_a = \Delta_a^{\text{opt}}$ and assume the red-sideband detuning resonance condition. It is revealed in Fig. 2(a) that no squeezing is generated near $G_a \sim 0$, or it is very weak. However, Fig.2(b) shows a large degree of squeezing generated even for $G_a = 0$ around the optimal acoustic resonance Δ_a^{opt} . This feature reveals how the synthetic gauge induces the squeezing even if the BSBS effect is not supported in the system. Moreover, it could be seen that the squeezing generated in the presence of $J_m \neq 0$ is stronger compared to the case when there is no mechanical coupling $J_m = 0$. To get further insight into the enhancement of the squeezing through the synthetic gauge, we study the mechanical position variance against the variation of both J_m and θ , as displayed in Fig.3(a). On the other hand, corresponding study for the effective phonon number is depicted in Fig.3(b). It should be noted that the effective phonon number corresponding to the mechanical oscillator n_{eff}^m can also be expressed in term of the V_{ij} elements, and it yields,

$$n_{eff}^m = \frac{1}{2} (V_{55}e^{-2r} + V_{66}e^{2r} - 1). \quad (18)$$

It can be seen from Figure 3(a,b) that both variance and

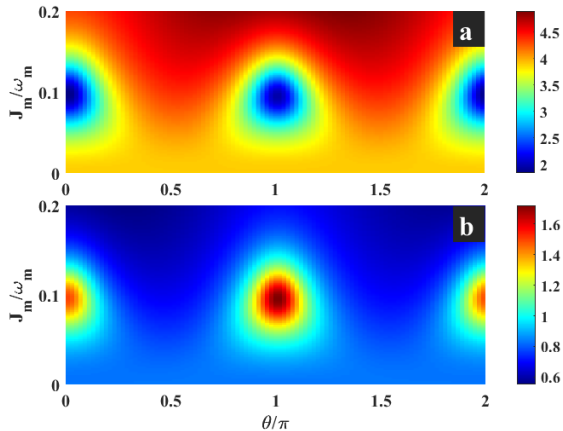


FIG. 3: (a) Mechanical position variance (Equation 17) and (b) effective (mechanical) phonon number (Equation 18) versus J_m and θ . Optimal squeezing parameters deduced from Figure 2 are used: $G_m = 0.15\omega_m$, $G_a = 0.124\omega_m$, and Δ_a^{opt} . The others parameters are similar to the ones in Figure 2.

phonon number are modulated along the θ direction. For

$J_m \leq 5 \times 10^{-2}\omega_m$, the effect of the phase θ is negligible. However, for $J_m > 5 \times 10^{-2}\omega_m$, the variance (Figure 3a) exhibits peaks at $\theta \equiv (n + \frac{1}{2})\pi$ and dips for $\theta \equiv n\pi$, n being an integer. This feature shows that significant squeezing is generated at $\theta \equiv (n + \frac{1}{2})\pi$. This also corresponds to an effective minimum phonon number as expected in Figure 3b (see near $J_m \sim 0.1\omega_m$ for instance). By paying attention to the colorbars of these figures, it can be figured out that with an increase in mechanical coupling J_m , the mechanical resonator is getting cooled down significantly resulting in stronger degree of squeezing. These figures point out the crucial role played by both J_m and θ regarding enhancement of squeezing in our proposal. To further reveal the oscillatory feature of the squeezing above discussed, we have extracted the position variance and phonon number from Figure 3 at $J_m \sim 0.1\omega_m$, and that is displayed in Appendix B.

Next, we investigate the role of synthetic gauge in enhancing the squeezing of the position quadrature. We take specific parameters in the (G_m, G_a) space, and in Fig. 4 depict how the position variance varies with γ_a, n_{th} and η . The left and right columns in Figure 4 depict the mechanical position variance plotted over the same variable for $J_m = 0$ and $J_m = 0.1\omega_m$, respectively. The first interesting parameter considered here is the Brillouin acoustic decay rate γ_a . The BSBS process involved in our proposal relies on the fact that $\gamma_a \gg \kappa (\gg \gamma_m)$. Therefore, it is crucial to point out the impact of this condition on the squeezing generation as shown in Figure 4(a,b). Without the mechanical coupling ($J_m = 0$), Figure 4a shows how the variance increases rapidly and reaches a saturation limit above $\gamma_a \gg \kappa = 2 \times 10^{-2}\omega_m$ as expected. Above this BSBS condition, the position variance settles on a sort of plateau, where the acoustic decay rate does no longer affect the behavior of the generated squeezing. This regime could be of great interests for quantum technologies involving squeezing such as quantum information processing, quantum sensing and metrology, and quantum computing. By considering the synthetic gauge ($J_m \neq 0$), Figure 4b shows a great enhancement of the degree of squeezing (from 0 to near 5dB) compared to when $J_m = 0$ (compare Figure 4a to Figure 4b). Despite the fact that the position variance behaves with almost the same shape in both Figure 4(a,b), it is worth to mention that the merit of the synthetic gauge has been to push the limit of the generated squeezing beyond the 3dB. Furthermore, these figures show that the more the couplings (G_m, G_a) are enhanced, better is the degree of the squeezing (see Appendix B for a large view). In Figure 4c, we have plotted the position variance over the thermal phonon mechanical excitation. The shadow area depicts the region below the 3dB. It can be seen that when $G_a = 0$, there is only a short window where the squeezing is above the 3dB (full line) compared to when $G_a \neq 0$ (dashed line). This feature reveals the key role played by the BSBS effect, which suppresses the heating processes in the system [44]. This BSBS effect is further reinforced through the gap between the two lines in Figure 4c, showing how $G_a \neq 0$ has improved the degree of squeezing compared to the case $G_a = 0$. By taking into account the synthetic gauge, we observe in Figure 4d that the gap between the cases $G_a = 0$ and $G_a \neq 0$ has been efficiently reduced. Indeed, the squeez-

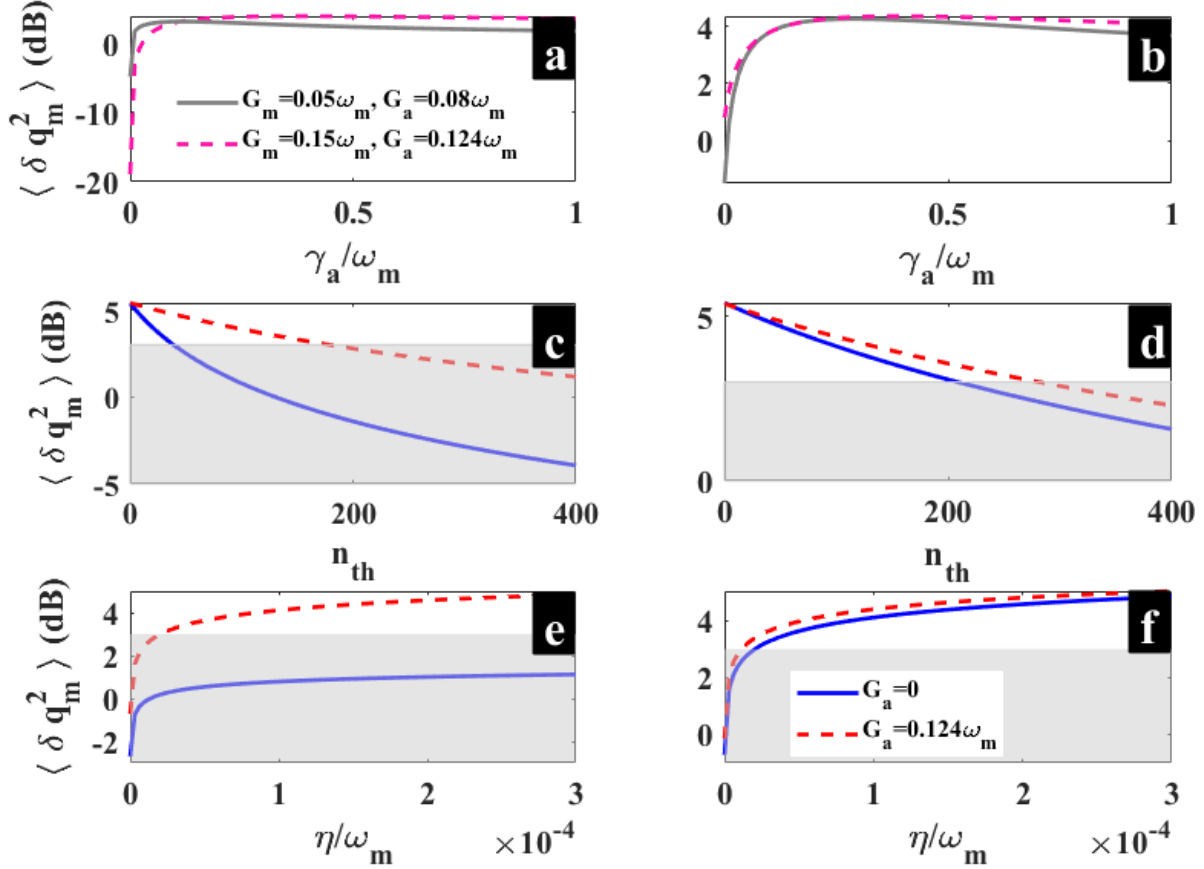


FIG. 4: Left and right column depicts the same quantities, which are plotted for $J_m = 0$ and $J_m = 0.1\omega_m$, respectively. (a,b) display the position variance of the mechanical resonator over the Brillouin acoustic decay rate γ_a for two specific couples of points (G_a, G_m) : $(0.05\omega_m, 0.08\omega_m)$ for the full line, and $(0.15\omega_m, 0.124\omega_m)$ for the dashed line. (c,d) analyze the robustness of the mechanical position variance versus the thermal noise n_{th} . (e,f) figure out the behavior of the mechanical position variance versus the Duffing coefficient η . In (c-f), the full line is for $G_a = 0$ and the dashed line is for $G_a = 0.124\omega_m$. The rest of the parameters are the same as in Figure 2.

ing generated for $G_a = 0$ follows almost the one generated for $G_a \neq 0$, and they stay longer beyond the 3dB compared to what is shown in Figure 4d. This confirms that the synthetic gauge contributes to suppress the heating channels, inducing strong squeezing even for $G_a = 0$, as earlier discussed in Figure 2. Furthermore, it can be observed that squeezing is somehow less prone to the affect of thermal phonons in the presence of synthetic gauge. In Figure 4(e,f), we display the mechanical position variance versus the Duffing nonlinear coefficient η . These figures show how the variance sharply increases for weak values of η , and settles quickly to a plateau like a saturation limit. However, it can be observed that the synthetic gauge bridges the gap between the cases $G_a = 0$ and $G_a \neq 0$ as previously discussed. Moreover, Figure 4e shows how the degree of the generated squeezing for $G_a = 0$ is below the 3dB, while it exceeds this limit for $J_m \neq 0$ as depicted in Figure 4f. Once again, this highlights the merit of the synthetic gauge that induces a strong squeezing even for $G_a = 0$ in our proposal as shown in Figure 2.

In Fig. 5(a) and (d) we exhibit the Wigner function distribu-

tion for the squeezed state generated for some specific parameters. Owing to the Gaussian nature of the quantum noise, our linearized system can be described through a single Gaussian Wigner function in the steady state defined as [28]

$$W(u_m) = \frac{1}{2\pi\sqrt{\det[V_m]}} \exp\left[-\frac{u_m^T V_m^{-1} u_m}{2}\right], \quad (19)$$

where $u_m = (\delta q_m, \delta p_m)^T$ is the column vector of the mechanical fluctuations and V_m stands for the covariance matrix for the mechanical mode. The left column in Figure 5 depicts the Wigner function distribution of the mechanical resonator (Figure 5a), the mechanical position variance (Figure 5b) and the mechanical momentum variance (Figure 5c) for the synthetic modulation phase of $\theta = 0$. Similarly, the right column displays the same quantities at $\theta = \frac{\pi}{2}$ i.e., the Wigner function distribution (Figure 5d), the position variance (Figure 5e) and the momentum variance (Figure 5f). These figures have been plotted in the long time limit so that the system has reached its steady state. Moreover, these figures have been extracted from Figure 3a for the mechanical coupling strength

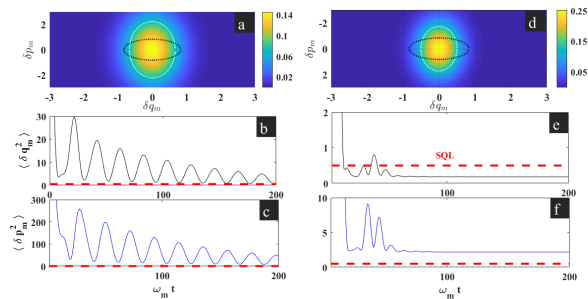


FIG. 5: Wigner function distributions and dynamic of mechanical variances. Left column depicts Wigner function (a), position variance (b) and the momentum variance (c) at $J_m = 0.1\omega_m$, and $\theta = 0$. Right column depicts Wigner function (d), position variance (e) and the momentum variance (f) at $J_m = 0.1\omega_m$, and $\theta = \pi/2$. These figures are extracted from the feature displayed in Figure 3. The other parameters are the same as in Figure 2.

fixed at $J_m = 0.1\omega_m$. In Figure 5(a,d), the contour represented by a dark circle depicts the related coherent state, while the shrunken and expanded shape bounded by the white ellipse features the corresponding generated squeezed state. As predicted from Figure 3a, the Wigner function at $\theta = 0$ (Figure 5a) shows less squeezing as compared to when $\theta = \pi/2$ (Figure 5d). Moreover, these Wigner function distributions confirm the squeezing along the position direction, while the quantum fluctuation is transferred to the momentum direction which is amplified. To further analyze these observations, we have plotted the dynamical time-evolution of the involved variances. As expected, both position and momentum dynamical evolution at $\theta = 0$ clearly show no squeezing (Figure 5(b,c)), which is revealed by an oscillatory behavior above the Standard Quantum Limit (SQL). However, we can qualitatively observe that there is less amount of noise along the position direction compared to the momentum direction as predicted by the corresponding Wigner distribution (Figure 5a). For $\theta = \pi/2$, however, Figure 5e shows squeezing in position quadrature below the SQL, while its corresponding momentum is far above the SQL, revealing that quantum fluctuation has been amplified along this direction as predicted from Figure 5d. From the above analysis, it can be seen that our Wigner function distribution together with the dynamical evolution of the variances agree well with the synthetic magnetism squeezing enhancement pointed out in Figure 3. This work provides an efficient scheme towards enhancement of squeezing beyond 3dB in optomechanical system that is based on the backward stimulated Brillouin scattering effect. The generated squeezing under this scheme is robust enough against thermal noise compared to the case without the synthetic magnetism. This investigation can be extended to electromechanical systems and hybrid opto-electromechanical systems.

IV. CONCLUSION

We have investigated the synthetic magnetism effect inducing mechanical squeezing enhancement in an optomechanical system, which hosts a backward stimulated Brillouin scattering process. Our model system consists of an acoustic mode that couples to two optical modes through the BSBS process, and a nonlinear mechanical oscillator that couples to the two optical modes through the standard optomechanical radiation pressure. A mechanical coupling, with a strength J_m that is modulated through a phase θ , is connecting the acoustic and mechanical modes, which induces a synthetic magnetism in our proposal. Without this synthetic magnetism, there is a given amount of squeezing that is generated in the system. This squeezing is mainly induced by the BSBS process, and is fragile against thermal noise. When the synthetic magnetism is accounted, the degree of the generated squeezing is greatly enhanced and goes far beyond the 3dB. Moreover, this large induced squeezing persists even when the system is free from the BSBS process. Furthermore, this generated squeezing is robust enough against thermal noise compared to the case without synthetic magnetism. Another merit of the synthetic magnetism in our proposal is revealed through the peaks and dips of both squeezing magnitude and mechanical effective phonon number depending on the modulation phase of the mechanical coupling. This oscillatory feature is reminiscent of a sudden death and revival of squeezing phenomenon, which can be used to maintain a desired magnitude of squeezing by tuning the phase θ . Our work sheds light on a flexible scheme that can be used to generate a large amount of mechanical squeezing, far beyond the 3dB limit. Our scheme can be implemented in optical and microwaves cavities, as well as in hybrid optomechanical systems. Such a generated squeezed states can be useful for a range of quantum applications including quantum information processing, quantum sensing and metrology, and the recent development in quantum computing.

Acknowledgments

This work has been carried out under the Iso-Lomso Fellowship at Stellenbosch Institute for Advanced Study (STIAS), Wallenberg Research Centre at Stellenbosch University, Stellenbosch 7600, South Africa. S. Agasti wishes to acknowledge the European Union H2020 MSCA; Project number: 101065991 (acronym: SingletSQL) for supporting the work. A.K. Sarma acknowledges the STARS scheme, MoE, government of India (Proposal ID 2023-0161). K.S. Nisar is grateful to the funding from Prince Sat-tam bin Abdulaziz University, Saudi Arabia project number (PSAU/2024/R/1445). The authors are thankful to the Deanship of Graduate Studies and Scientific Research at University of Bisha for supporting this work through the Fast-Track Research Support Program.

Appendix A: Effective Hamiltonian

The Hamiltonian that describes the system considered by us is given by,

$$\begin{aligned}
H = & \sum_{j=1,2} \omega_{c_j} a_j^\dagger a_j + \omega_a b_a^\dagger b_a + \omega_m b_m^\dagger b_m - \sum_{j=1,2} g_{m,a} a_j^\dagger a_j (b_m + b_m^\dagger) \\
& + \frac{\eta}{2} (b_m + b_m^\dagger)^4 + J_m (e^{i\theta} b_a^\dagger b_m + e^{-i\theta} b_a b_m^\dagger) \\
& + \sum_{j=1,2} iE_j (a_j^\dagger e^{-i\omega_{p_j} t} - a_j e^{i\omega_{p_j} t}) - g_a (a_1^\dagger a_2 b_a + a_1 a_2^\dagger b_a^\dagger).
\end{aligned} \tag{A1}$$

The total Hamiltonian of the hybrid system in a frame rotating with the laser frequency ω_{p_j} is given by:

$$\begin{aligned}
H' = & - \sum_{j=1,2} \Delta_j a_j^\dagger a_j + \Delta_a b_a^\dagger b_a + \omega_m b_m^\dagger b_m - \sum_{j=1,2} g_{m,a} a_j^\dagger a_j (b_m + b_m^\dagger) \\
& + \frac{\eta}{2} (b_m + b_m^\dagger)^4 + J_m (e^{i\theta} b_a^\dagger b_m + e^{-i\theta} b_a b_m^\dagger) \\
& + iE_1 (a_1^\dagger - a_1) + iE_2 (a_2^\dagger - a_2) - g_a (a_1^\dagger a_2 b_a + a_1 a_2^\dagger b_a^\dagger),
\end{aligned} \tag{A2}$$

with $\Delta_j = \omega_{p_j} - \omega_{c_j}$, and $\Delta_a = \omega_a + \omega_{p_2} - \omega_{p_1}$. By considering that the control field a_2 is strong enough compared to a_1 , it can be treated classically by deriving its steady-state as,

$$\dot{a}_2 = i[H', a_2], \tag{A3}$$

$$\begin{aligned}
& = (i\Delta_2 - \frac{\kappa_2}{2}) a_2 + i g_m a_2 (b_m + b_m^\dagger) + E_2 + i g_a a_1 b_a^\dagger \\
& = (i\Delta_2' - \frac{\kappa_2}{2}) a_2 + E_2 + i g_a a_1 b_a^\dagger,
\end{aligned} \tag{A4}$$

with $\Delta_2' = \Delta_2 + g_m a_2 (b_m + b_m^\dagger)$. The steady-state solution ($\dot{a}_2 = 0$) yields,

$$\alpha_2 \sim \frac{-E_2}{i\Delta_2' - \frac{\kappa_2}{2}} \quad \text{or} \quad |\alpha_2| \sim \frac{E_2}{\sqrt{\Delta_2'^2 + \frac{\kappa_2^2}{4}}}. \tag{A5}$$

By substituting this expression in the rest of the Hamiltonian in Equation A2, we get the following reduced Hamiltonian,

$$\begin{aligned}
H' = & -\Delta_1 a_1^\dagger a_1 + \Delta_a b_a^\dagger b_a + \omega_m b_m^\dagger b_m - g_m a_1^\dagger a_1 (b_m + b_m^\dagger) \\
& + \frac{\eta}{2} (b_m + b_m^\dagger)^4 + J_m (e^{i\theta} b_a^\dagger b_m + e^{-i\theta} b_a b_m^\dagger) \\
& + iE_1 (a_1^\dagger - a_1) - G_a (a_1^\dagger b_a + a_1 b_a^\dagger),
\end{aligned} \tag{A6}$$

where the acoustic effective coupling is $G_a = g_a \alpha_2$ as mentioned in the main text.

Appendix B: Oscillatory behavior and effect of the effective couplings

This section highlights some phenomena aforementioned in the main text related to Figure 3 and Figure 4. Indeed, it was mentioned that the position variance and the phonon

number displayed in Figure 3 exhibit sort of oscillatory behavior depending on the synthetic phase θ around the phonon hopping rate $J_m = 0.1\omega_m$. Moreover, it was pointed out that these two quantities are out of phase with each other over θ . Figure 6a depicts the position variance while Figure 6b shows variation of effective phonon numbers against phase θ . These depictions are extracted from Figure 3a and Figure 3b at $J_m = 0.1\omega_m$, respectively. As expected, it can be clearly seen how these two quantities exhibit oscillatory features and are out of phase.

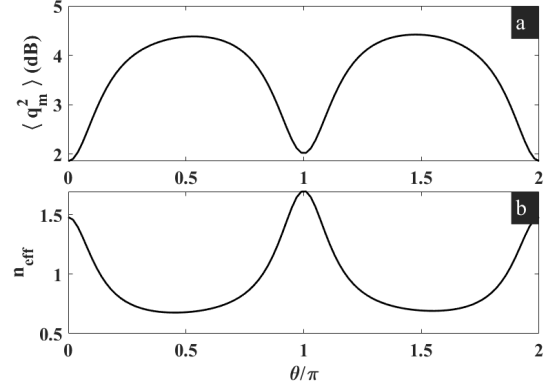


FIG. 6: Mechanical position variance (a) and effective phonon number (b) (extracted from Figure 3 at $J_m = 0.1\omega_m$) against variation of phase θ . The other parameters are the same as in Figure 2.

In Figure 4, it has been pointed out that as the effective coupling G_a and G_m are enhanced, the strength of squeezing gets enhanced as well. To get a clearer view of that feature, Figure 7 displays the mechanical position variance in G_a and G_m space for $J_m = 0$ (a) and $J_m = 0.1\omega_m$ (b). As it can be seen in both figures, the squeezing gets stronger and stronger as the strength of the two effective couplings increases. This justifies our statement aforementioned in the main text. Moreover, by paying attention to the colorbars in Figure 7, it appears that the squeezing is enhanced as the synthetic magnetism is accounted in the system, i.e., $J_m \neq 0$ and $\theta = \pi/2$. This can be seen by comparing the couple of points highlighted in Figure 7 for instance.

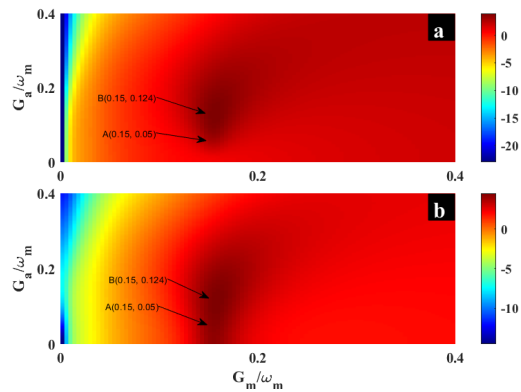


FIG. 7: Squeezing degree of the mechanical position variance in G_a and G_m space for $J_m = 0$ (a) and $J_m = 0.1\omega_m$ (b). The rest of the parameters are the same used in Figure 2.

-
- [1] G. Wendin, Reports on Progress in Physics **80**, 106001 (2017), ISSN 1361-6633.
- [2] S. Slussarenko and G. J. Pryde, Applied Physics Reviews **6**, 041303 (2019), ISSN 1931-9401.
- [3] N. Meher and S. Sivakumar, The European Physical Journal Plus **137**, 985 (2022), ISSN 2190-5444.
- [4] C. Degen, F. Reinhard, and P. Cappellaro, Reviews of Modern Physics **89** (2017), ISSN 1539-0756.
- [5] E. Polino, M. Valeri, N. Spagnolo, and F. Sciarrino, AVS Quantum Science **2**, 024703 (2020).
- [6] B. Stray, A. Lamb, A. Kaushik, J. Vovrosh, A. Rodgers, J. Winch, F. Hayati, D. Boddice, A. Stabrawa, A. Niggebaum, et al., Nature **602**, 590 (2022), ISSN 1476-4687.
- [7] M. Barbieri, PRX Quantum **3**, 010202 (2022).
- [8] M. Zidan, H. Eleuch, and M. Abdel-Aty, Results in Physics **21**, 103536 (2021), ISSN 2211-3797.
- [9] F. Arute, K. Arya, R. Babbush, D. Bacon, J. C. Bardin, R. Barends, R. Biswas, S. Boixo, F. G. S. L. Brandao, D. A. Buell, et al., Nature **574**, 505 (2019), ISSN 1476-4687.
- [10] H.-S. Zhong, H. Wang, Y.-H. Deng, M.-C. Chen, L.-C. Peng, Y.-H. Luo, J. Qin, D. Wu, X. Ding, Y. Hu, et al., Science **370**, 1460 (2020), ISSN 1095-9203.
- [11] H.-S. Zhong, Y.-H. Deng, J. Qin, H. Wang, M.-C. Chen, L.-C. Peng, Y.-H. Luo, D. Wu, S.-Q. Gong, H. Su, et al., Physical Review Letters **127** (2021), ISSN 1079-7114.
- [12] M. Aspelmeyer, T. J. Kippenberg, and F. Marquardt, Reviews of Modern Physics **86**, 1391 (2014), ISSN 1539-0756.
- [13] D. P. Foulla, P. Djourwé, S. T. Kingni, and S. G. N. Engo, Physical Review A **95**, 123 (2017).
- [14] R. Riedinger, A. Wallucks, I. Marinković, C. Löschnauer, M. Aspelmeyer, S. Hong, and S. Gröblacher, Nature **556**, 473 (2018), ISSN 1476-4687.
- [15] C. Tchodimou, P. Djourwe, and S. G. N. Engo, Physical Review A **96** (2017).
- [16] S. Kotler, G. A. Peterson, E. Shojaei, F. Lecocq, K. Cicak, A. Kwiatkowski, S. Geller, S. Glancy, E. Knill, R. W. Simmonds, et al., Science **372**, 622 (2021), ISSN 1095-9203.
- [17] S. Chakraborty and A. K. Sarma, Physical Review A **100**, 063846 (2019), ISSN 2469-9934.
- [18] D. R. K. Massembele, P. Djourwé, A. K. Sarma, and S. G. N. Engo, arXiv (2024).
- [19] Y. Xia, A. R. Agrawal, C. M. Pluchar, A. J. Brady, Z. Liu, Q. Zhuang, D. J. Wilson, and Z. Zhang, Nature Photonics **17**, 470 (2023), ISSN 1749-4893.
- [20] A. J. Brady, X. Chen, Y. Xia, J. Manley, M. Dey Chowdhury, K. Xiao, Z. Liu, R. Harnik, D. J. Wilson, Z. Zhang, et al., Communications Physics **6** (2023), ISSN 2399-3650.
- [21] H. Vahlbruch, M. Mehmet, K. Danzmann, and R. Schnabel, Physical Review Letters **117** (2016), ISSN 1079-7114.
- [22] W. Qin, A. Miranowicz, and F. Nori, Physical Review Letters **129** (2022), ISSN 1079-7114.
- [23] J. B. Clark, F. Lecocq, R. W. Simmonds, J. Aumentado, and J. D. Teufel, Nature **541**, 191 (2017), ISSN 1476-4687.
- [24] P. Djourwé, J. H. T. Mbé, S. G. N. Engo, and P. Wofo, Physical Review A **86**, 043816 (2012).
- [25] J. Aasi, J. Abadie, B. P. Abbott, R. Abbott, T. D. Abbott, M. R. Abernathy, C. Adams, T. Adams, P. Addesso, R. X. Adhikari, et al., Nature Photonics **7**, 613 (2013), ISSN 1749-4893.
- [26] B. P. A. et al., Physical Review Letters **116**, 061102 (2016).
- [27] W. Qin, A. Miranowicz, H. Jing, and F. Nori, Physical Review Letters **127** (2021), ISSN 1079-7114.
- [28] P. Banerjee, S. Kalita, and A. K. Sarma, Journal of the Optical Society of America B **40**, 1398 (2023), ISSN 1520-8540.
- [29] P. Djourwe, Y. Pennec, and B. Djafari-Rouhani, Physical Review Applied **12**, 024002 (2019).
- [30] S. M. Tchounda, P. Djourwé, S. N. Engo, and B. Djafari-Rouhani, Physical Review Applied **19**, 064016 (2023), ISSN 2331-7019.
- [31] P. Djourwé, M. Asjad, Y. Pennec, D. Dutykh, and B. Djafari-Rouhani, arXiv (2023).
- [32] K. Stannigel, P. Komar, S. J. M. Habraken, S. D. Bennett, M. D. Lukin, P. Zoller, and P. Rabl, Physical Review Letters **109** (2012), ISSN 1079-7114.
- [33] G. Madiot, R. C. Ng, G. Arregui, O. Florez, M. Albrechtsen,

- S. Stobbe, P. D. García, and C. M. Sotomayor-Torres, *Physical Review Letters* **130** (2023), ISSN 1079-7114.
- [34] H. Ren, T. Shah, H. Pfeifer, C. Brendel, V. Peano, F. Marquardt, and O. Painter, *Nature Communications* **13** (2022), ISSN 2041-1723.
- [35] M. J. Woolley and A. A. Clerk, *Physical Review A* **89** (2014), ISSN 1094-1622.
- [36] E. E. Wollman, C. U. Lei, A. J. Weinstein, J. Suh, A. Kronwald, F. Marquardt, A. A. Clerk, and K. C. Schwab, *Science* **349**, 952 (2015), ISSN 1095-9203.
- [37] C. Lei, A. Weinstein, J. Suh, E. Wollman, A. Kronwald, F. Marquardt, A. Clerk, and K. Schwab, *Physical Review Letters* **117** (2016), ISSN 1079-7114.
- [38] M. Schmidt, S. Kessler, V. Peano, O. Painter, and F. Marquardt, *Optica* **2**, 635 (2015).
- [39] K. Fang, Z. Yu, and S. Fan, *Nature Photonics* **6**, 782 (2012).
- [40] C. Brendel, V. Peano, O. J. Painter, and F. Marquardt, *Proceedings of the National Academy of Sciences* **114** (2017).
- [41] J. P. Mathew, J. del Pino, and E. Verhagen, *Nature Nanotechnology* **15**, 198 (2020).
- [42] X. Wang, H.-R. Li, and F.-L. Li, *New Journal of Physics* **22**, 033037 (2020).
- [43] D.-G. Lai, J.-Q. Liao, A. Miranowicz, and F. Nori, *Physical Review Letters* **129**, 063602 (2022).
- [44] Z. Shen, Y.-L. Zhang, C.-L. Zou, G.-C. Guo, and C.-H. Dong, *Phys. Rev. Lett.* **126**, 163604 (2021).
- [45] P. Djourwé, H. Alphonse, S. Abbagari, S. Doka, and S. N. Engo, *Chaos, Solitons and Fractals* **170**, 113333 (2023), ISSN 0960-0779.